applied optics

Modeling and validation of uniform large-area optical coating deposition on a rotating drum using microwave plasma reactive sputtering

CHENG LI,[1] SHIGENG SONG,[1] DES GIBSON,[1,*] DAVID CHILD,[1] HIN ON CHU,[1] AND EWAN WADDELL[2]

[1]Institute of Thin Films, Sensors and Imaging, Scottish Universities Physics Alliance, School of Engineering & Computing, University of the West of Scotland, Paisley, Scotland, UK
[2]Thin Film Solutions Ltd., Block 7, Kelvin Campus, West of Scotland Science Park, Maryhill Road, Glasgow G20 0SP, Scotland, UK
*Corresponding author: Des.Gibson@uws.ac.uk

Received 30 August 2016; revised 17 October 2016; accepted 18 October 2016; posted 18 October 2016 (Doc. ID 274929); published 15 November 2016

Magnetron sputter deposition onto a rotating drum is a method applied to high-throughput large-area optical coating deposition, where film physical thickness uniformity is an important parameter. Techniques have been developed, such as masking/substrate movement, in order to improve sputtered film uniformity. In this study, a model is described and validated for predicting film uniformity. Experimental data show excellent agreement with modeled simulations, with and without a modified sputtering mask. Practical application is demonstrated in maximizing uniformity over an individual substrate size of 100 cm^2 for a high-optical-density visible/near-infrared dual-band laser protection filter. © 2016 Optical Society of America

OCIS codes: (310.1860) Deposition and fabrication; (310.3840) Materials and process characterization.

http://dx.doi.org/10.1364/AO.56.000C65

1. INTRODUCTION

Sputter deposition typically involves a magnetron source, where a target material is bombarded with an ionized gas. These magnetrons do not eject material uniformly as the bombardment is controlled by the magnetic field configuration [1]. This can result in nonuniform coatings, where approaches to alleviate this can involve use of a target mask, substrate rotation, or both.

Uniform coatings are particularly important in optical applications, such as antireflection coatings [2,3], optical filters [4,5], plasmonics [6], and high laser damage and/or laser protection filters [7,8]. Optical filters are generally made using multilayers of typically two materials, with high refractive index contrast and control of each layer thickness (typical required control $< \pm 1\%$) to achieve required optical filter performance. Niobia (high refractive index) and silica or alumina (low refractive index) are common oxides typically used in visible/near-infrared precision multilayer optical coatings.

Development of vacuum coating technology and equipment for coating onto planar substrates has greatly improved, with a focus on maximizing throughput achieved by improving large-area uniformity [9]. One method in particular is the sputter deposition onto a rotating drum to maximize coating area and throughput [10,11]. The film thickness distribution obtained from sputter magnetrons directly influences the usable substrate size and hence throughput and yield per run. Moreover, in precision work, the film thickness distribution and control is critical to achieving required optical filter spectral characteristic. Researchers and production engineers require a fast method to accurately model and predict such mask modifications. Mask design based on an empirical approach can be difficult, time consuming, and expensive. There are limited reports in the literature that specifically use both experiments and theory toward sputter mask design [12–14], especially when it is a drum-based sputtering system as opposed to the planetary substrate rotation setup.

In this study, a MathCAD-15-based magnetron sputtering simulation, through a uniformity mask, is used to optimize the mask spatial design and thickness uniformity at the substrate plane. Two complementary approaches have been used to obtain a mesh for the simulation: the real spatial profile measurement of the sputter target surface and through tangential magnetic flux measurements at the sputter target surface.

Masks were subsequently optimized for enhanced film uniformity. This work demonstrates use of the model to maximize uniformity of multilayer coatings for use in optical filter applications. A specific example used is a visible/near-infrared dual-band laser protection optical filter, providing high optical density (OD) (>7) over an extended angle of incidence range (0°–30°). The individual substrate size was 100 cm^2, with sixteen substrates distributed around the drum circumference.

2. EXPERIMENTAL

Room temperature deposition was carried out using a microwave-plasma-assisted pulsed DC reactive sputtering system, shown schematically in Fig. 1. The system was equipped with mechanical masking in front of the sputter targets to achieve enhanced surface uniformity across the substrate. The deposition system utilizes a drum rotating on a horizontal axis, where deposition of each layer can be achieved with multiple passes across a rectangular planar pulsed DC magnetron source, with subsequent exposure to a microwave plasma region.

Drum rotation speed is such that one to two monolayers are deposited per pass across the magnetron target, with full oxidation of the sputtered metal or semiconductor, at room temperature, and with the monolayer in the separate microwave plasma region. The deposition rate was monitored using a quartz crystal microbalance. The critical deposition rate for this process has been previously investigated [15]. BK7 glass (10 cm × 10 cm) was used as the substrate for these experiments. Two magnetron targets of niobium and aluminum were used to fabricate Nb_2O_5 and Al_2O_3 for the high/low refractive index, respectively. Single-layer films of each material were deposited onto BK7 glass. Dual-band laser protection filter specifications were high optical density (>7), 532 nm/755 to 810 nm, and wide angle of incidence (0°–30°). These were fabricated by depositing multilayers of niobia and alumina. Film uniformity was optimized by adjusting the mask geometry. The customized mask was fixed to the magnetron flange. This is illustrated in Fig. 2, where the mask blocks certain paths of sputtered material to the substrate. Mask design is based on the model shown in Section 3. The magnetic field distribution of the magnetron target was measured using a magnetometer.

An Aquila nkd-8000 spectrometer was used to measure the optical transmission, at 10° incidence angle with *S* polarization, over a 350 to 1100 nm spectral range. This measurement is background compensated. The optical film thickness, refractive index, and extinction coefficient (*n* and *k*) were derived from curve fitting using the Cauchy model. Typical n/k values at 550 nm for niobia and alumina are 2.348/0.0002 and 1.674/0.0001, respectively. Optical density measurements were acquired at 532 nm over the required angle of incidence range. These measurements were provided by Spica Technologies Inc.

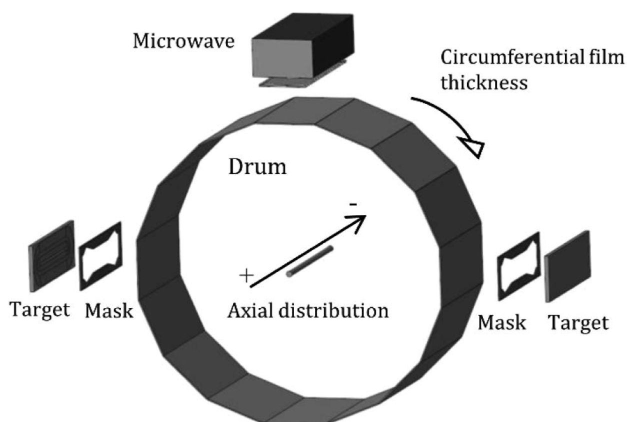

Fig. 1. Schematic of the microwave-plasma-assisted pulsed DC sputter system. This shows targets, masks, the microwave, circumferential direction, and axial distribution direction.

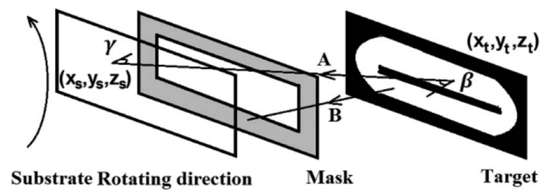

Fig. 2. Schematic of the sputtering geometry, where the substrate is mounted on a rotating drum, β is the ejected particle flux emission angle to the target surface normal, and γ is the deposited particle flux incident angle to the substrate surface normal. On path A, the particle reaches the substrate, and on path B, the particle is blocked by the mask. This is generated directly from the measurement of the target erosion track profile.

3. THICKNESS DISTRIBUTION MODELING

A simulation model to design the mask was established using MathCAD 15. This takes into account the substrates on the rotating drum, sputtering targets, and a mask with predefined shape, as illustrated in Fig. 2.

In order to optimize the mask to achieve high uniformity over a large area, the sputtering yield, angular distribution of the ejected particles of the target, the mask restriction function (which determines whether particles can pass through the mask or not, this will be described as the *Passrate*), the arriving angle of sputtered particles on the substrate, as well as the substrate movement need to be taken into account. The thickness simulation (see Section 3.B), as described in Fig. 3, uses several derived parameters to generate a target and substrate mesh. This is then used to define the mask shape function, which includes the terms "*Trackyield*" and "*Passrate*." These terms are defined in Sections 3.A and 3.B.

A. Sputtering Yield

Sputtering yield is a function of bombardment particles, magnetic field, cathode voltage, and gas pressure. During deposition, gas pressure and cathode voltage remain constant; this can be assumed uniform across the whole target surface. Thus, for this calculation, the gas pressure and cathode voltage

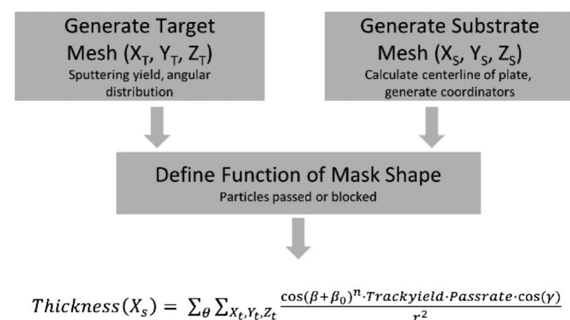

$$Thickness(X_s) = \sum_\theta \sum_{X_t,Y_t,Z_t} \frac{\cos(\beta+\beta_0)^n \cdot Trackyield \cdot Passrate \cdot \cos(\gamma)}{r^2}$$

Fig. 3. Flow chart of how the thickness will be simulated. The "Trackyield" describes the 2D sputtering data array from the target. "Passrate" is a binary, 0 or 1, that describes whether the sputtered material reaches the substrate or is blocked by the mask.

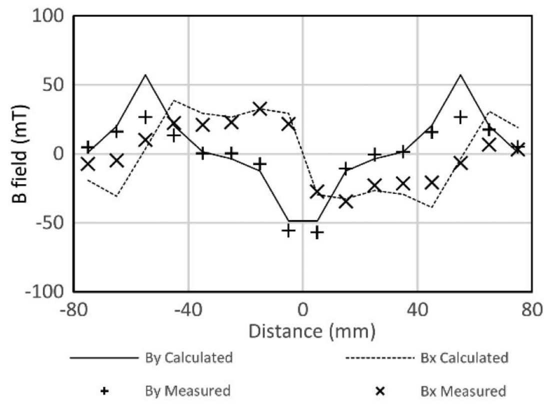

Fig. 4. Magnetic field, B, was obtained at different locations on a cross section of the magnetron.

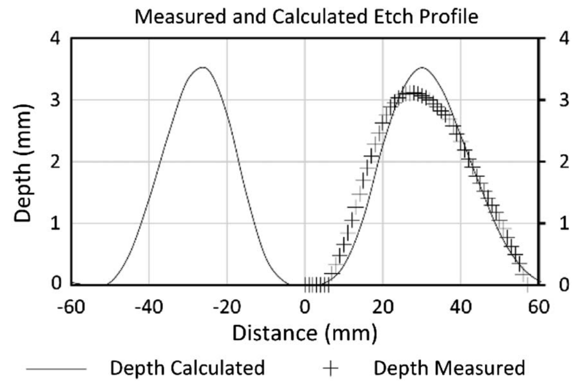

Fig. 6. Comparison of calculated and measured values of track erosion over a cross section of the linear magnetron.

parameters are not considered. Magnetic field B_{tan}, which is tangential to the cathode target surface, contributes to electron confinement, plasma generation, and is highly nonuniform across the target surface. According to the investigation by Goree and Sheridan [16], using a Monte Carlo simulation method, there is a trade-off when the magnetic field is lower than a certain value and ionization will be saturated. Between these two critical magnetic fields, the ionization efficiency almost remains a linear relation to the log of the dimensionless magnetic field β_{field} [Eq. (1)]. Therefore, the sputtering yield distribution on the target surface is not uniform; this is reflected by the erosion track profile. The magnetic field is given by

$$\beta_{\text{field}} = \sqrt{e/2m}(a/V_{\text{dis}}^{1/2})B_{\text{tan}}. \quad (1)$$

Here, e and m are the electron charge and mass, respectively, and a is the distance from the target center to where the magnetic field is tangential to the target surface. V_{dis} is the cathode bias. Thus, the relative yield distribution of the target surface can be obtained by measuring the tangential magnetic field B_{tan}. Figure 4 shows the measured B_{tan}. B_{tan} measurements can then be used to calculate the sputter yield.

Another method to obtain the relative target surface sputtering yield is to measure the erosion track profile directly. Figure 5 shows a quarter of a magnetron target track. This method gives a direct measure of the erosion rate.

These two methods can derive the sputtering yield, as mentioned before; the log β is linearly related to the ionization efficiency. Thus, the sputtering yields can be derived through

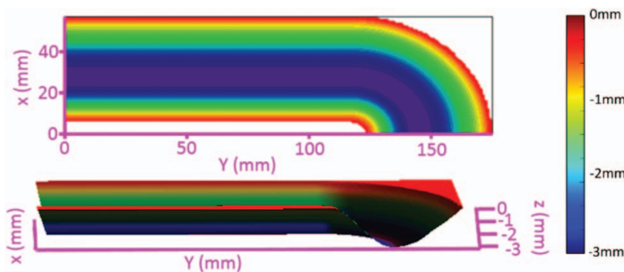

Fig. 5. Quarter of the target is shown; this displays the target track erosion, obtained by direct measurements. From red to violet, the color scale gives depth information of the track.

target surface measurements of B_{tan}. Figure 6 is a comparison between these two methods; the section is assumed to have linear 2D geometry. Thus, edge effects are not taken into account. Both methods show good agreement, thus implying that either approach can be used for deriving the etch profile. In this work, the measured depth profile will be used as this is the most accurate profile, which will validate the calculated approach.

The measured profile data will be used to generate a two-dimensional data array of relative sputtering yield. For convenience, we define this surface sputtering yield data array as a function of "Trackyield."

B. Sputtering Angular Distribution

In the thickness distribution simulation, the sputtered atoms angular distribution needs to be considered. The emission angle distribution is a function of the bombardment beam incident angle. In our research, both polycrystalline (Nb) and crystalline (Al) target materials were employed. For polycrystalline materials, the sputter yield tends to increase with increased deviation from the target normal, until reaching a maximum. For crystalline materials, this behavior is more complicated; some pronounced minima and maxima depend on the crystalline structure. Minima are observed for bombardment along closely packed directions, where ions may be redirected into open channels without undergoing collision events that are dramatic enough to cause emission of atoms or molecules from the surface [17]. In this investigation, however, pulsed DC magnetron sputtering was used. The incident angles of bombardment ions are mostly at normal angle to the target surface [18,19]. By considering particle collisions and a turbulent electric field, a mean incident angle of 7.95° to the surface normal has been obtained using Monte Carlo simulation by Goeckner *et al.* [19]. Therefore, the variation of bombardment ion incident angle is negligible for the simulation reported in this work.

The general function of angular distribution for ejected particles is required for magnetron sputtering. For crystalline targets, the angular distribution of sputtered particles is related to the crystal structure of the sputter target, as shown by Sigmund [17]. Through the measurement of the Ag (100) crystal target emission pattern, bombarded by 100 eV Hg ions, this information is useful for simulating crystalline Si target sputtering. The angular distribution of sputtered particles for

polycrystalline targets is also of interest. Here we will use the results from Martynenko for angular distribution of sputtered atoms of polycrystalline targets, using magnetron sputtering [20]. According to their experimental results, targets can be divided into two groups based on the shape of the angular distribution. Using the maximum emission angle to the target surface normal: 0° and approximately 30°, each with functions of $f(\beta) = A\cos^n\beta$ and $f(\beta) = A\cos^n\beta - B\cos^m\beta$ applied, respectively, where A, B, n, and m are all adjustable parameters (for more details, see Ref. [20]). To simplify calculations, a simple function is used in our simulation:

$$f(\beta) = \cos(\beta + \beta_0)^n. \quad (2)$$

Here, β_0 is the angle of maximum emission, and n is an approximation parameter.

C. Thickness Simulation

Additional parameters are needed for this simulation. From Fig. 2, sputtered particles leaving the target surface then travel to substrate surface. As each point on the sputter target can be considered as point sources, the number of particles arriving on the substrate surface is proportional to $1/r^2$, where r is the distance between the point (X_t, Y_t, Z_t) on the target and the point (X_s, Y_s, Z_s) on the substrate. The projection effect also needs to be considered. Thus, a factor of $\cos(\gamma)$ is introduced, where γ is the angle between the deposition beam and the substrate surface normal, as shown in Fig. 2.

Finally, the mask is taken into account. A function describing the mask shape is used to carry out geometrical analysis to determine whether the sputtered particles will reach the substrate surface or be blocked by the mask. In this case, the value of the result will be either 1 or 0; this value is defined as the "Passrate." The function describing the process where the particle is sputtered from a point (X_t, Y_t, Z_t) on the sputter target and then travels to the point (X_s, Y_s, Z_s) on the substrate is shown as follows [Eq. (3)]:

$$\text{Probability} = \frac{\cos(\beta + \beta_0)^n \cdot \text{Trackyield} \cdot \text{Passrate} \cdot \cos(\gamma)}{r^2}. \quad (3)$$

This mathematical calculation method is used to divide target fine mesh structures with coordinates of (X_t, Y_t, Z_t). At one particular point on the substrate, the relative thickness of the coating can be obtained from the sum of the probability of all target mesh elements. As the film thickness along the circumference of the rotating drum is uniform, only the central line of the drum plate (which is parallel to the drum rotating axis) is used for calculation to optimize mask design. Due to drum rotation, the particular point at the centerline of the plate moves along the circumference. As shown in Fig. 2, we may construct a specific data set for calculations using coordinates $(X_s, Y_{s0}\text{-}R\sin\theta, Zs_0\text{-}R\cos\theta)$ for the point X_s at the centerline and moved to the θ angle. Here, (X_s, Y_{s0}, Z_{s0}) are the coordinates on the rotating axis. The final relative thickness at point X_s can be obtained by integrating θ for a range of $(-\theta_0, \theta_0)$. The final equation for thickness simulation is

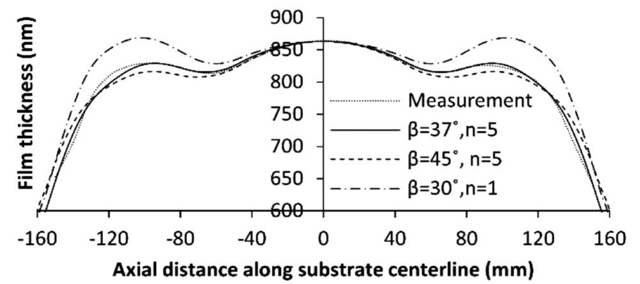

Fig. 7. Original uniformity mask and simulated depositions are used to obtain values of β and n.

$$\text{Thickness}(X_s) = \sum_{\theta}\sum_{X_t,Y_t,Z_t} \times \frac{\cos(\beta + \beta_0)^n \cdot \text{Trackyield} \cdot \text{Passrate} \cdot \cos(\gamma)}{r^2}. \quad (4)$$

Using Eq. (4) and a predefined shape function of the mask, numerical results of the thickness simulation were obtained.

4. MASK OPTIMIZATION

The mask design was optimized based on single-layer depositions of niobia. As seen in Fig. 7, the optically measured thickness uniformity (from the central 50 mm) was ±2.3%. From this, the parameters n and β were fitted for Nb.

In the MathCAD simulation, with β from 30° to 45° and n between 1 and 10, the best fit was found for $\beta = 37°$ and $n = 5$. This was then used to revise the function "Passrate" and reconfigure the mask shape, with a predicted uniformity of 0.3%. This predicted uniformity was limited by mask manufacturing constraints. A further deposition of Nb_2O_5 using the redesigned mask improved the uniformity from the original ±2.3% to ±0.5%. While the change in film uniformity improves with the change in mask shape, the measured uniformity is less than the predicted uniformity by 0.2%. Figure 8 shows this difference, which is attributed to the simplification of straight line modifications as well as the difficulty in removing very small amounts of mask material *in situ*.

In order to examine the difference between polycrystalline (Nb) and crystalline (Al) target emission patterns, the optimized mask for Nb_2O_5 was used for the deposition of Al_2O_3. It was found that these Al_2O_3 films exhibited an improved

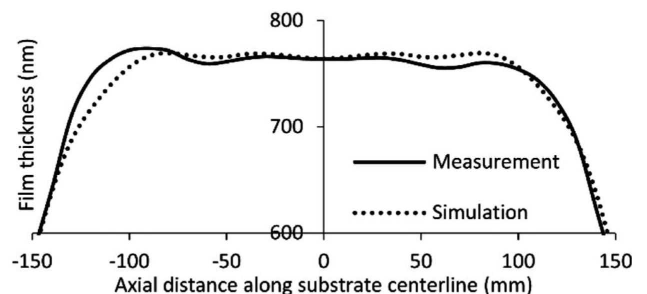

Fig. 8. Comparison of simulated deposition, using derived constants, with measured deposition using the simplified optimized mask.

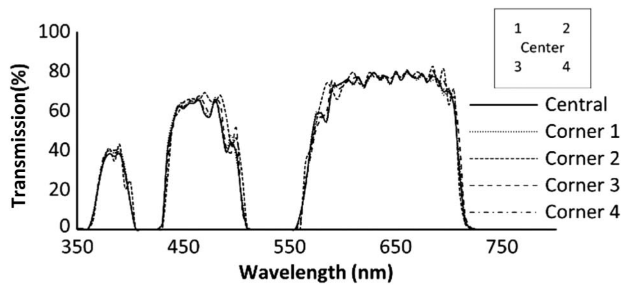

Fig. 9. Comparison of spectral transmission of the center and four corner points (100 mm × 100 mm plate) demonstrating uniformity of ±0.3%.

uniformity from ±2.4% to ±0.8%. This shows that the optimized mask may be suitable for other materials. However, because a different magnetron and crystal structure were used, further study is required to determine the exact cause of this discrepancy.

5. APPLICATIONS: MULTILAYER COATING

Laser protection filters, deposited with multilayer thin films, require high precision of each individual layer (typical required control $< \pm 1\%$). The optimized masks were used for both Nb_2O_5 and Al_2O_3 deposition as the high (2.34) and low (1.67) refractive index materials, respectively. It was found that the filter uniformity improved from ±1.4% to ±0.3% for a 100 cm^2 area. The spectral transmission measurement of five different locations on the filter showed good consistency in their spectral characteristics. Figure 9 displays the relative locations and their respective transmission spectra. Measured bandpass spectral edge positions are consistent at the five measurement positions.

The observed multilayer coating uniformity of ±0.3% appears to initially contradict the single-layer uniformities reported in Section 4: Nb_2O_5 and Al_2O_3 measured uniformities of ±0.5 and ±0.8, respectively.

In this case, the physical thickness uniformity of the high/low refractive index layers compensates the optical thickness (refractive index x physical thickness). This results in an effective uniformity of ±0.3% for the Nb_2O_5/Al_2O_3 pair, explaining the improved multilayer result. Variation in uniformity across the sixteen 100 cm^2 substrates loaded around the drum circumference was within measurement error. Optical density (OD) measurements for the laser protection filters showed an average optical density of 7.45 across 0°–30°. This was measured over six samples, with a standard deviation of ±0.6%.

Agreement between theoretical design and measured performance indicates ±0.7% control of layer thickness was achieved. Achieved thickness uniformity over the 100 cm^2 area is ±0.3%, with average OD = 7.45 over an angle of incidence range of 0° to 30° and normal incidence integrated visible photonics transmittance = 32%.

6. CONCLUSIONS

A simulation model was developed to predict mask shape and achieve uniform coatings on a rotating-drum-based sputtering method. The B_{tan} measured on the target surface is highly nonlinear and nonsymmetrical, as can be seen in the lack of symmetry in Figs. 4, 5, and 6. Despite this and the restrictions introduced to simplify mask manufacturing, the predicted uniformity closely matches the deposited films. These are significantly better than previous results, where uniformity improved from ±2.4% to ±0.8% for alumina and from ±2.3% to ±0.5% of niobia.

As this improvement is similar for crystalline and polycrystalline materials, this implies that the emission pattern is not a significant factor in mask design and that geometric parameters are the primary influence, as shown by Zhang [14]. Deposition of a dual-band (532/755 to 810 nm), high-optical-density (>7), and wide-angle-of-incidence (0°–30°) laser protection filter has been demonstrated over a 100 cm^2 substrate area with measured uniformity of ±0.3%. Enhanced multilayer uniformity, compared with single layers, is explained by a compensatory effect in the optical thickness due to opposite sense physical thickness uniformity in the high/low refractive index films.

Agreement between theoretical design and measured performance indicate ±0.7% control of layer thickness was achieved over a 100 cm^2 area and across 16 plates distributed around the rotating drum.

Acknowledgment. We would like to thank Andy Bunyan, Gerry O'Hare, and Jim Orr for their input to this project, as well as Spica Technology Inc. supplying optical density data, and the Scottish Universities Physics Alliance (SUPA) for support.

REFERENCES

1. J. A. Thornton, "Magnetron sputtering: basic physics and application to cylindrical magnetrons," J. Vac. Sci. Technol. **15**, 171–177 (1978).
2. J. Szczyrbowski, G. Bräuer, G. Teschner, and A. Zmelty, "Antireflective coatings on large scale substrates produced by reactive twin-magnetron sputtering," J. Non-Cryst. Solids **218**, 25–29 (1997).
3. C. Guo, M. Kong, C. Liu, and B. Li, "Optimization of thickness uniformity of optical coatings on a conical substrate in a planetary rotation system," Appl. Opt. **52**, B26–B32 (2013).
4. J. C. Travis, N. K. Winchester, and M. V. Smith, "Determination of the transmittance uniformity of optical filter standard reference materials," J. Res. Natl. Inst. Stand. Technol. **100**, 241–256 (1995).
5. J.-C. Hsu, "Analysis of the thickness uniformity improved by using wire masks for coating optical bandpass filters," Appl. Opt. **53**, 1474–1480 (2014).
6. D. Feng, W. Zhou, X. Qiao, and J. Albert, "High resolution fiber optic surface plasmon resonance sensors with single-sided gold coatings," Opt. Express **24**, 16456–16464 (2016).
7. M. Alvisi, "HfO_2 films with high laser damage threshold," Thin Solid Films **358**, 250–258 (2000).
8. M. Alvisi, "Laser damage dependence on structural and optical properties of ion-assisted HfO_2 thin films," Thin Solid Films **396**, 44–52 (2001).
9. J. Xu, H. Fan, W. Liu, and L. Hang, "Large-area uniform hydrogen-free diamond-like carbon films prepared by unbalanced magnetron sputtering for infrared anti-reflection coatings," Diam. Relat. Mater. **17**, 194–198 (2008).
10. C. Z. Jiang, J. Q. Zhu, J. C. Han, P. Lei, and X. B. Yin, "Uniform film in large areas deposited by magnetron sputtering with a small target," Surf. Coat. Technol. **229**, 222–225 (2013).
11. V. K. Jayaraman, Y. M. Kuwabara, A. M. Álvarez, and M. L. O. Amador, "Importance of substrate rotation speed on the growth of

homogeneous ZnO thin films by reactive sputtering," Mater. Lett. **169**, 1–4 (2016).
12. J. Sun, W. Zhang, K. Yi, and J. Shao, "Optimization of thickness uniformity of coatings on spherical substrates using shadow masks in a planetary rotation system," Chin. Opt. Lett. **12**, 53101–53104 (2014).
13. C. Liu, M. Kong, C. Guo, W. Gao, and B. Li, "Theoretical design of shadowing masks for uniform coatings on spherical substrates in planetary rotation systems," Opt. Express **20**, 23790–23797 (2012).
14. Y. Zhang, Q. Song, and Z. Sun, "Research on thin film thickness uniformity for deposition of rectangular planar sputtering target," Phys. Procedia **32**, 903–913 (2012).
15. S. Song and F. Placido, "In-situ investigation of spontaneous and plasma-enhanced oxidation of AlN film surfaces," Appl. Phys. Lett. **99**, 121901 (2011).
16. J. Goree and T. E. Sheridan, "Magnetic field dependence of sputtering magnetron efficiency," Appl. Phys. Lett. **59**, 1052–1054 (1991).
17. P. Sigmund, "Fundamental processes in sputtering of atoms and molecules (SPUT92)," in *Symposium on the Occasion of the 250th Anniversary of the Royal Danish Academy of Sciences and Letters, Invited Reviews* (Kongelige Danske videnskabernes selskab, 1993), Vol. **43**.
18. C. H. Shon and J. K. Lee, "Modeling of magnetron sputtering plasmas," Appl. Surf. Sci. **192**, 258–269 (2002).
19. M. J. Goeckner, J. A. Goree, and T. E. Sheridan, "Monte Carlo simulation of ions in a magnetron plasma," IEEE Trans. Plasma Sci. **19**, 301–308 (1991).
20. Y. V. Martynenko, A. V. Rogov, and V. I. Shul'ga, "Angular distribution of atoms during the magnetron sputtering of polycrystalline targets," Tech. Phys. **57**, 439–444 (2012).

148.191.228.21 {ts '2017-02-01 02:58:34'}